PHYSICAL REVIEW B **87**, 121102(R) (2013)

Periodic Anderson model with electron-phonon correlated conduction band

Peng Zhang,[1] Peter Reis,[1] Ka-Ming Tam,[1] Mark Jarrell,[1] Juana Moreno,[1] Fakher Assaad,[2] and A. K. McMahan[3]
[1]*Department of Physics and Astronomy, Louisiana State University, Baton Rouge, Louisiana 70803, USA*
[2]*Institute for Theoretical Physics and Astrophysics, University of Würzburg, 97070 Würzburg, Germany*
[3]*Lawrence Livermore National Laboratory, University of California, Livermore, California 94550, USA*
(Received 6 September 2012; published 4 March 2013)

This Rapid Communication reports dynamical mean-field calculations for the periodic Anderson model in which the conduction band is coupled to phonons. Motivated in part by recent attention to the role of phonons in the γ-α transition in Ce, this model yields a rich and unexpected phase diagram which is of intrinsic interest. Specifically, above a critical value of the electron-phonon interaction, a first-order transition with two coexisting phases develops in the temperature-hybridization plane, which terminates at a second-order critical point. The coexisting phases display the familiar Kondo screened and local-moment character, yet they also exhibit pronounced polaronic and bipolaronic properties, respectively.

DOI: 10.1103/PhysRevB.87.121102 PACS number(s): 71.27.+a, 71.10.Fd, 71.38.−k

The periodic Anderson model (PAM) and its impurity variant have played pivotal roles in elucidating the nature of Kondo screening as the techniques of many-body theory have improved.[1–3] Perhaps its most noted application has been the Kondo volume collapse scenario for understanding the unique isostructural γ-α transition in Ce, with its very large 15% volume change.[4,5] The relative merits of this perspective versus the Mott transition scenario[6] are still under debate, although both focus on critical $4f$-electron correlation effects, and the finite temperature predictions are rather similar.[7] The PAM exhibits a smooth crossover from a local-moment region with Curie Weiss susceptibility (γ-like) to a region with Kondo screened $4f$ moments and a paramagnetic susceptibility (α-like), as a function of increasing hybridization between the $4f$ and valence electrons.[8] Although the PAM also predicts a first-order transition given proper consideration of the Maxwell construction of the free energy versus volume curves,[4] it requires modifications like some f-f hybridization[9] so as to display a first-order phase transition with two coexisting phases at the same hybridization in the temperature-hybridization plane.

Over the past decade attention in the Ce literature has shifted to an appreciation that a significant fraction of the total entropy change across the transition may be due to phonons.[10–16] However, studies focusing on the effect of phonons on the PAM are very limited.[17–21] Prior studies either are constrained to ground-state calculation or do not explore possible phase transitions in detail. To this end, we are motivated here to consider the PAM with Holstein phonons.[22,23] Since the coupling of phonons to the f electrons can lead to loss of local moments via electron condensation, we have chosen to couple the phonons to the conduction electrons in the present work. We find that the electron-phonon interaction above a critical strength induces a first-order transition in the temperature-hybridization plane for the PAM-Holstein model. Strikingly the electron-phonon interaction also creates polaronic behavior in the Kondo screened phase and bipolaronic behavior in the local-moment phase. This intriguing phase diagram is explored in the remainder of the present Rapid Communication.

The Hamiltonian of the PAM-Holstein model is

$$\begin{aligned} H &= H_0 + H_U + H_{e-\mathrm{ph}}, \\ H_0 &= -t \sum_{\langle i,j\rangle,\sigma} (c^\dagger_{i,\sigma} c_{j,\sigma} + c^\dagger_{j,\sigma} c_{i,\sigma}) + \epsilon_f \sum_{i,\sigma} f^\dagger_{i,\sigma} f_{i,\sigma} \\ &\quad + V \sum_{i,\sigma} (c^\dagger_{i,\sigma} f_{i,\sigma} + f^\dagger_{i,\sigma} c_{i,\sigma}) + \sum_i \left(\frac{P_i^2}{2m} + \frac{1}{2} k X_i^2 \right), \\ H_U &= U \sum_i n^f_{i,\uparrow} n^f_{i,\downarrow}, \\ H_{e-\mathrm{ph}} &= g \sum_{i,\sigma} n^c_{i,\sigma} X_i, \end{aligned} \tag{1}$$

where $c_{i,\sigma}$, $c^\dagger_{i,\sigma}$ ($f_{i,\sigma}$, $f^\dagger_{i,\sigma}$) are the creation and annihilation operators of the conduction (f level) at site i and spin σ; $n^c_{i,\sigma} = c^\dagger_{i,\sigma} c_{i,\sigma}$ and $n^f_{i,\sigma} = f^\dagger_{i,\sigma} f_{i,\sigma}$ represent the occupation of the c and f electrons, respectively; t is the nearest-neighbor hopping; ϵ_f is the on-site energy of the f level; V is the hybridization between conduction and localized electrons; the on-site Hubbard interaction is U; g is the electron-phonon coupling; X_i is the lattice displacement at site i, and P_i is its conjugate momentum.

Due to the absence of experimental evidence for long-range ordering in Ce volume collapse in the primary range of interest at room temperature and above, together with the smooth Fermi surface we choose, dynamical mean-field theory (DMFT)[24] is employed in our simulation. We use a hypercubic lattice in infinite dimensions with Gaussian density of states $D(\epsilon) = \frac{1}{\sqrt{\pi} W} e^{-\left(\frac{\epsilon}{W}\right)^2}$. The bandwidth W is set to 1 as the unit of energy. In Ce the Fermi energy is about 6000 K and the Debye frequency is 110–160 K,[10,16] therefore we set the phonon frequency $\omega_0 = 0.01$ at 1% of bandwidth. The Hubbard interaction is $U = 4.0$. The total electronic density is fixed at $n = 1.8$ by tuning the chemical potential, and we adjust ϵ_f so that $n_f = 1$ at $T = 0.1$ to ensure that a local moment is present at high temperatures. Therefore all data we show are for $n_f \sim 1.0$ and $n_c \sim 0.8$. The continuous time quantum Monte Carlo,[25] generalized for electron-phonon coupling,[26] is employed as the impurity solver.

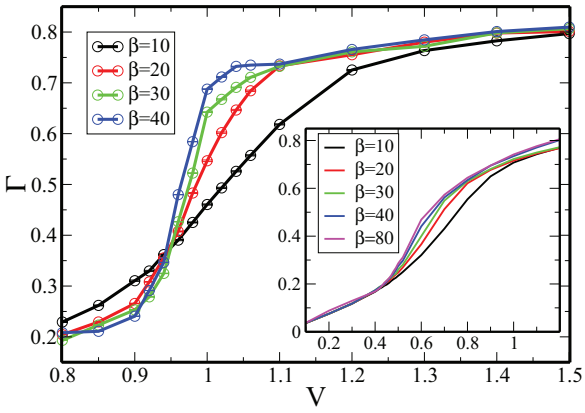

FIG. 1. (Color online) Isothermal scan of the hybridization factor $\Gamma = \langle c_0^+ f_0 + \text{H.c.}\rangle$ as a function of V at $g^2/2k = 1.0$. Γ increases monotonically with V. As the temperature decreases, Γ vs V becomes steeper with a diverging slope near $V_c \sim 0.96$. Inset: Isothermal scan of the hybridization factor Γ as a function of V at $g^2/2k = 0.49$. Notice that the critical behavior has disappeared.

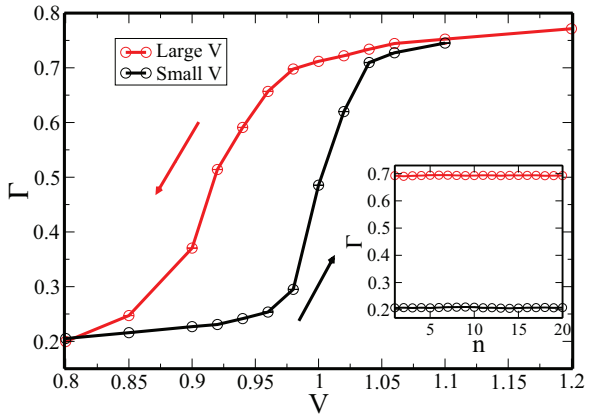

FIG. 2. (Color online) Hysteresis of Γ vs V for $T = 0.0167$, $g^2/2k = 1.0$. The black line represents the small V branch of the hysteresis for which the self-energy of the previous simulation is used to initiate the calculation for the next larger value of V. While the red line represents the large V branch where starting with $V = 1.2$, we use the output of the previous simulation to initiate the computation at the next lower value of V. Inset: Γ as a function of the DMFT iteration number n for $V = 0.96$, $T = 0.0167$. The black (red) symbols represent the small (large) V branches.

Figure 1 displays the local hybridization factor $\Gamma = \langle c_0^+ f_0 + \text{H.c.}\rangle$ (here zero denotes the impurity site) as a function of V for $g^2/2k = 1.0$ and different values of inverse temperature, β. As the temperature decreases, the slope of the Γ vs V curve becomes progressively larger, which indicates that the system is approaching a critical point. Interestingly, the curves approximately cross at a critical hybridization $V_c \sim 0.96$. The inset of Fig. 1 shows Γ vs V at $g^2/2k = 0.49$. Notice that for this value of coupling the slope does not become steeper as the temperature decreases, and the line crossing disappears. This indicates that the corresponding susceptibility reaches a plateau as a function of temperature. We believe $g^2/2k = 0.49$ is the lower bound for the critical value of the electron-phonon coupling. For any electron-phonon coupling smaller than 0.49, including PAM, the slope changing feature and consequently the critical behavior are lost.

When the temperature is further decreased to $T = 0.0167$ ($\beta = 60$), Γ vs V displays a hysteresis loop as shown in Fig. 2. The red line is obtained by starting at the large V side ($V = 1.2$) and using the output self-energy to initiate the simulation for the next smaller V. On the other hand, we obtain the black line by starting at $V = 0.8$ and using the output self-energy as the input for the next larger value of V. The coexistence of two solutions for the same value of V at $T = 0.0167$ is a direct evidence of a first-order phase transition. The absence of such a hysteresis at higher temperatures indicates that the first-order transition ends at a second-order terminus (V_c, T_c).

For the same parameters, $V = 0.96$, $g^2/2k = 1.0$, $\omega_0 = 0.01$, and $U = 4.0$, we also perform a series of isothermal scans on the chemical potential to study the relationship between the total electron density $n = n_c + n_f$ and the chemical potential μ. As long as the temperature is not below $T = 0.0167$, the compressibility $\frac{dn}{d\mu}$ shows no tendency to diverge. This indicates that the phase transition here is not compressibility driven.

In Fig. 3 we show the temperature times the local f-orbital spin susceptibility, $T \cdot \chi_s^{ff}$, versus temperature. As T approaches zero, $T \cdot \chi_s^{ff}$ is roughly constant for $V = 0.8$, while it goes to zero for $V = 1.2$. This indicates that at $V = 0.8$ the f electrons display a robust local moment and paramagnetic local susceptibility with $1/T$ dependence, while at $V = 1.2$ the f local moments are quenched. The inset of Fig. 3 shows the f-orbital density of states (DOS) at $T = 0.01$. Notice that at $V = 0.8$ there is a gap across the Fermi level, while at $V = 1.2$ a Kondo resonance peak appears. The screening of the local moment in the large V region is a consequence of the singlet formation between c and f electrons.

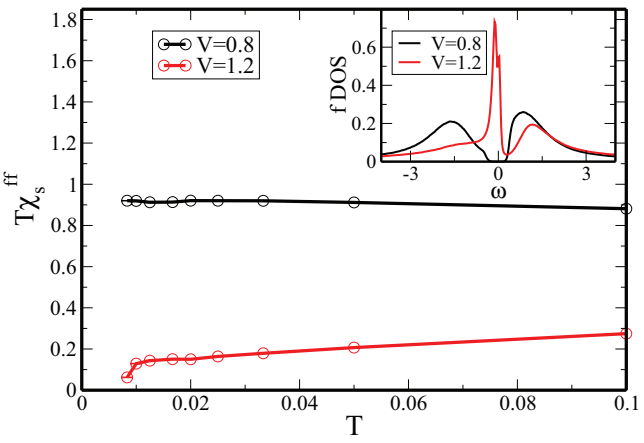

FIG. 3. (Color online) Temperature times the local f-orbital spin susceptibility, $T \cdot \chi_s^{ff}$, as a function of temperature for $g^2/2k = 1.0$. For $V = 0.8$ (black line), $T \cdot \chi_s^{ff}$ approaches a constant value as $T \to 0$, indicating an unscreened moment. For $V = 1.2$ (red line), $T \cdot \chi_s^{ff}$ converges to zero, indicating that the local moment is screened. Inset: The f-electron DOS at $T = 0.01$. The Kondo peak found for $V = 1.2$ (red line) but absent for $V = 0.8$ (black line) is consistent with the screening and unscreening scenarios in the main panel.

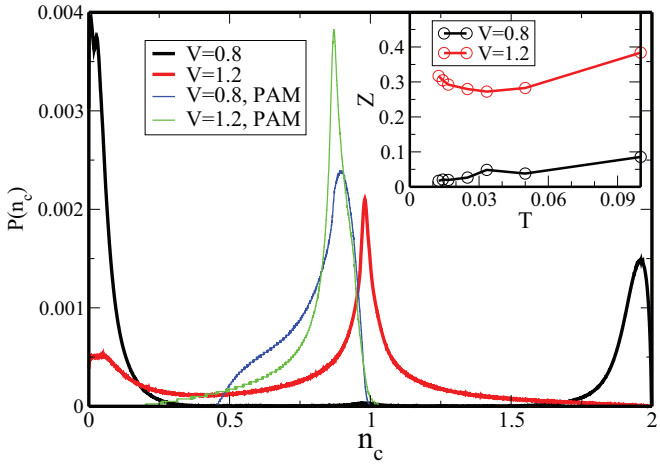

FIG. 4. (Color online) Occupancy distribution histogram of c-orbital $P(n_c)$ for $V = 0.8$ (black line) and 1.2 (red line), $T = 0.0167$, and $g^2/2k = 1.0$. For comparison, $P(n_c)$ of the PAM without electron-phonon coupling is plotted as well: $V = 0.8$ (blue line) and $V = 1.2$ (green line). Inset: Quasiparticle Z factor as a function of temperature for $V = 0.8$ (black line) and 1.2 (red line).

The main panel of Fig. 4 shows the occupancy distribution histogram of the c electrons, $P(n_c)$, at $T = 0.0167$. $P(n_c)$ has been used to illustrate bipolaron formation.[26] At $V = 0.8$ the c-orbital electrons are in a bipolaronic state, which is characterized by the oscillation between zero and double occupancy, while for $V = 1.2$ the c electrons are in a polaronic state, where the occupancy oscillates between zero and one. For the PAM, without electron-phonon coupling, the structure of $P(n_c)$ is totally different. Here there is only one peak at roughly the c-electron filling $n_c = 0.8$, and $P(n_c)$ quickly decays to zero for n_c away from this filling. In the inset, the quasiparticle fraction Z is plotted as a function of temperature. The quasiparticle fraction is calculated for the lower quasiparticle band at the Fermi level using a generalization of the single band formulation.[27] The main component of this approach is to make the replacement $\frac{dRe\Sigma(\omega)}{d\omega}|_{\omega=0} \approx \frac{\mathrm{Im}\Sigma(i\pi T)}{\pi T}$, which becomes exact at zero temperature. As $T \to 0$, Z goes to zero for $V = 0.8$, indicating non-Fermi-liquid behavior, while it converges to a finite value for $V = 1.2$, the signature of Fermi-liquid formation.

We find that this Kondo singlet to local-moment phase transition remains for a large range of parameters, like adjusting the total filling to $n = 1.6$, changing the Hubbard interaction to $U = 3.8$, and increasing the phonon frequency to $\omega_0 = 0.02$ and 0.05, while keeping $g^2/2k$ fixed. For these different parameters, we find that the isothermal Γ vs V curves still cross and their slopes diverge at a critical value of the hybridization, V_c, as the temperature is decreased. We also find that V_c changes roughly linearly with $g^2/2k$.

In Fig. 5(a) the time integrated local f-orbital spin-spin-correlation function, χ_s^{ff}, is plotted as a function of temperature for $V = 1.1, 1.2$, and 1.3. We identify the Kondo scale T_K as the energy where χ_s^{ff} falls to around half of its low-temperature value. We find that T_K changes very little as V increases, so the line V vs T_K should have a large slope. Figure 5(b) shows the time integrated local

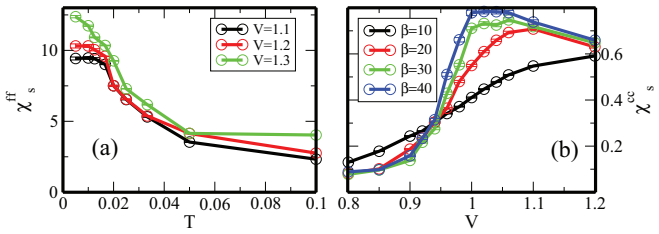

FIG. 5. (Color online) (a) The f-orbital time integrated local spin-spin correlation, χ_s^{ff}, as a function of temperature for $V = 1.1$, 1.2, and 1.3. (b) The c-orbital time integrated local spin-spin correlation function, χ_s^{cc}, as a function of V for different temperatures.

c-orbital spin-spin-correlation function, χ_s^{cc} vs V, at different temperatures, where large values reflect the c-electron spin degeneracy in the polaronic state in contrast to the small susceptibility for the spinless bipolarons. For $V < 0.96$ the curves almost overlap for all $T < 0.1$. In fact, the corresponding c-electron occupancy histograms (not shown) show an obvious bipolaronic double peak feature even at relatively high temperatures like $T = 0.1$. If we define T^* as the energy where bipolaron formation begins, then the line T^* vs V must be nearly horizontal.

We have also calculated the renormalized phonon frequency. At $T = 0.025$ it is roughly constant for hybridization $V > 0.96$; however, it drops precipitously for $V < 0.96$, decreasing by half when $V = 0.8$. This behavior softens with increasing temperature; e.g., a more gradual decrease begins for $V < 1.2$ at $T = 0.1$. This indicates an important temperature dependence of the phonon properties. Indeed, the analysis in Ref. 14 for Ce found that the temperature dependence of the phonons was a critical factor for obtaining a significant phonon contribution to the entropy change across the γ-α transition.[10–16]

Figure 6 is a schematic summary of our findings. Two phases, local-moment-bipolaron and Kondo singlet polaron, are separated by a first-order transition line, which terminates

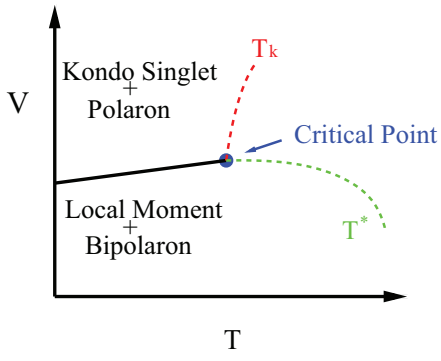

FIG. 6. (Color online) Schematic V vs T phase diagram. The solid black line represents the first-order phase transition, which separates the local-moment bipolaron phase for small hybridization V from the Kondo singlet polaron phase for large V. This first-order transition line terminates at a second-order critical point. The red dashed line coming out of the critical point represents the Kondo scale T_K, and the green dashed line represents the bipolaron energy scale T^*.

at a second-order critical point (V_c, T_c). The positive slope of the V vs T first-order transition line is a consequence of a Clausius-Clapeyron-like relation where hybridization V is the analog of pressure. There is no broken symmetry between these two phases, as we can move adiabatically from one to another by wandering around the critical point. Both phases are destroyed by increasing the temperature. In order to have such a first-order phase transition, the electron-phonon coupling on the c band must be larger than a certain critical value. The fact that the critical temperature is a function of electron-phonon coupling implies that the critical point touches zero temperature at some g_c, where the first-order phase transition becomes a quantum phase transition tuned by V.

The DMFT calculations for the Hubbard-Holstein Hamiltonian[28–30] allow us to comment on the difference between the Mott-Hubbard + phonon model and our PAM + phonon model. Both models predict a bipolaronic insulating phase at some finite g, although with different slopes as a function of increasing hybridization (f-f or f-valence). The fundamental topological difference is that for the Hubbard-Holstein model the γ phase (insulating) has a first-order transformation to the bipolaronic insulating phase with increasing g, while for the PAM-Holstein model the γ phase (local moment) can always be evolved continuously to the bipolaronic insulator phase.

In conclusion, when the conduction band of the PAM is coupled to phonons, one obtains a rich and unexpected phase diagram. Above a critical strength of the electron-phonon coupling a first-order transition with two coexisting phases develops in the temperature-hybridization plane. This transition terminates at a second-order critical point. These coexisting phases correspond to the familiar Kondo screened and local-moment regions of the PAM, yet they additionally exhibit pronounced polaronic and bipolaronic behavior, respectively. While the PAM and its impurity variant have been paradigms for the α-γ transition in Ce, additional electronic bands not considered here might be needed in a generalization of the present PAM-Holstein model to more completely explain the volume collapse. Nonetheless, the present results suggest that electron-phonon effects become more important in Ce at weaker hybridization (lower pressure), that there is profound temperature dependence to the phonons in the γ as distinct from the α phase, and that the polaronic effects seen here are consistent with the superconductivity observed[31] in Ce at much lower temperatures [$T < \mathrm{O}\,(1\ \mathrm{K})$] at pressures above 2 G Pa. That the effects seen here are more striking in the γ phase is no accident, as only for this phase are the characteristic phonon energies (Debye temperature)[16] comparable to the critical energy scale of hybridization between $4f$ and valence electrons (Kondo temperature).[4,5]

We thank Thomas Pruschke for valuable discussions. This work is supported by NSF Grant No. OISE-0952300 (P.Z., P.R., and J.M.), Department of Energy (DOE) SciDAC Grant No. DE-FC02-06ER25792 (K.M.T. and M.J.), and at Lawrence Livermore National Laboratory by DOE Contract No. DE-AC52-07NA27344 (A.K.M). This work used the Extreme Science and Engineering Discovery Environment, which is supported by NSF Grant No. DMR100007.

[1] A. C. Hewson, *The Kondo Problem to Heavy Fermions* (Cambridge University Press, New York, 1993).
[2] M. Jarrell, H. Akhlaghpour, and T. Pruschke, Phys. Rev. Lett. **70**, 1670 (1993).
[3] Z. Gulácsi and D. Vollhardt, Phys. Rev. Lett. **91**, 186401 (2003).
[4] J. W. Allen and R. M. Martin, Phys. Rev. Lett. **49**, 1106 (1982); M. Lavagna, C. Lacroix, and M. Cyrot, Phys. Lett. A **90**, 210 (1982).
[5] J. W. Allen and L. Z. Liu, Phys. Rev. B **46**, 5047 (1992).
[6] B. Johansson, Philos. Mag. **30**, 469 (1974).
[7] K. Held, C. Huscroft, R. T. Scalettar, and A. K. McMahan, Phys. Rev. Lett. **85**, 373 (2000).
[8] C. Huscroft, A. K. McMahan, and R. T. Scalettar, Phys. Rev. Lett. **82**, 2342 (1999).
[9] L. de' Medici, A. Georges, G. Kotliar, and S. Biermann, Phys. Rev. Lett. **95**, 066402 (2005).
[10] M. E. Manley *et al.*, Phys. Rev. B **67**, 014103 (2003).
[11] I.-K. Jeong, T. W. Darling, M. J. Graf, Th. Proffen, R. H. Heffner, Y. Lee, T. Vogt, and J. D. Jorgensen, Phys. Rev. Lett. **92**, 105702 (2004).
[12] F. Decremps, D. Antonangeli, B. Amadon, and G. Schmerber, Phys. Rev. B **80**, 132103 (2009).
[13] D. Antonangeli *et al.*, High Press. Res. **30**, 151 (2010).
[14] M. J. Lipp, D. Jackson, H. Cynn, C. Aracne, W. J. Evans, and A. K. McMahan, Phys. Rev. Lett. **101**, 165703 (2008).
[15] B. Johansson, A. V. Ruban, and I. A. Abrikosov, Phys. Rev. Lett. **102**, 189601 (2009).
[16] M. Krisch *et al.*, Proc. Natl. Acad. Sci. USA **108**, 9342 (2011).
[17] K. Mitsumoto and Y. Ōno, Physica C **426**, 330 (2005).
[18] T. Hotta, J. Phys. Soc. Jpn. **76**, 084702 (2007).
[19] R. Nourafkan and N. Nafari, Phys. Rev. B **79**, 075122 (2009).
[20] M. Raczkowski, P. Zhang, F. F. Assaad, T. Pruschke, and M. Jarrell, Phys. Rev. B **81**, 054444 (2010).
[21] O. Bodensiek *et al.*, J. Phys.: Condens. Matter **23**, 094212 (2011).
[22] T. Holstein, Ann. Phys. (NY) **8**, 325 (1959); **8**, 343 (1959).
[23] J. K. Freericks, M. Jarrell, and D. J. Scalapino, Phys. Rev. B **48**, 6302 (1993).
[24] A. Georges, G. Kotliar, W. Krauth, and M. J. Rozenberg, Rev. Mod. Phys. **68**, 13 (1996).
[25] A. N. Rubtsov, V. V. Savkin, and A. I. Lichtenstein, Phys. Rev. B **72**, 035122 (2005).
[26] F. F. Assaad and T. C. Lang, Phys. Rev. B **76**, 035116 (2007).
[27] D. W. Hess and J. W. Serene, J. Phys. Chem. Solids **52**, 1385 (1991).
[28] A. Deppeler and A. J. Millis, Phys. Rev. B **65**, 100301 (2002); **65**, 224301 (2002); P. Werner and A. J. Millis, Phys. Rev. Lett. **99**, 146404 (2007).
[29] W. Koller, D. Meyer, Y. Ōno, and A. C. Hewson, Europhys. Lett. **66**, 559 (2004); W. Koller, A. C. Hewson, and D. M. Edwards, Phys. Rev. Lett. **95**, 256401 (2005).
[30] M. Capone, G. Sangiovanni, C. Castellani, C. Di Castro, and M. Grilli, Phys. Rev. Lett. **92**, 106401 (2004); M. Capone, P. Carta, and S. Ciuchi, Phys. Rev. B **74**, 045106 (2006).
[31] See, e.g., I. Loa, E. I. Isaev, M. I. McMahon, D. Y. Kim, B. Johansson, A. Bosak, and M. Krisch, Phys. Rev. Lett. **108**, 045502 (2012).